RSC Advances

ROYAL SOCIETY OF CHEMISTRY

www.rsc.org/advances

Preparation of reduced graphene oxide hydrogel by Ni ions and its use in supercapacitor electrode

Van Hoang Luan, Jin Suk Chung, Seung Hyun Hur*

School of Chemical Engineering, University of Ulsan, Daehak-ro 93, Nam-gu, Ulsan 680-749, South Korea

*Corresponding authors: shhur@ulsan.ac.kr

ABSTRACT

A three-dimensional (3D) reduced graphene oxide hydrogel (rGOH) was prepared by the hydrothermal synthesis based on the electrostatic force and chemical reaction between graphene oxide (GO) and Ni ions in a nickel acetate solution. The Ni-rGOH fabricated in this study exhibited highly increased surface area than that of NiO nanoparticles owing to the formation of 3D networks. After the reduction of functional groups in Ni-GOH, Ni-rGOH showed highly enhanced capacitance (351 F g^{-1}) at a charge/discharge current density of 0.625 A g^{-1} and 90% capacitance retention after 1,000 cycles. The energy density of Ni-rGOH was 175.5 Wh kg^{-1} at a power density of 1.125 kW kg^{-1}, while maintaining a high-energy density of 118 Wh kg^{-1} at a power density of 4.5 kW kg^{-1}

Keywords: graphene oxide hydrogel; nickel oxide; supercapacitor.

1. Introduction

In recent years, electrochemical capacitors (ECs), also known as supercapacitors, have been extensively explored owing to their high power density, long cycle life, short charging time, and excellent safety.[1–4] Among four parts including positive electrode, negative electrode, separator, and aqueous electrolyte, the electrode material is considered as the most important unit to enhance the properties of supercapacitors.

In general, the carbon materials such as activated carbon, graphene, and carbon nanotube can be used as active materials for the electrodes of ECs owing to their high electrical conductivity and surface properties.[5, 6] To achieve high capacitance, surface area, pore size distribution, and pore volume should be well designed and controlled to maximize the ion adsorptions and minimize the resistance of ion transport. A recent study showed that reduced graphene oxide hydrogel (rGOH), a 3D structured material with the special properties such as light weight, high surface area, and pore volume can be effectively used as the electrode materials for power storage applications.[7-9]

Another strategy to enhance the capacitance of ECs is using transition metals that can increase the capacitance by the redox reaction with their oxidized forms. Nickel oxide (NiO) is one example of the transition metals with high redox capacity in aqueous electrolyte. Moreover, when it is hybridized with rGO, the capacitance can be highly increased owing to the high theoretical specific capacitance of NiO and excellent electrical conductivity of rGO.[10, 11]

In this study, highly porous hybrid 3D structures composed of NiO and rGOH were fabricated by the crosslinking between Ni ions and functional groups of graphene oxides (GO) using a simple one-pot hydrothermal process followed by the high-temperature annealing. The chemical bonds between GO and Ni were formed during the hydrothermal process, and GO and

$Ni(OH)_2$ were transformed to rGO and NiO, respectively, during the high-temperature annealing. The supercapacitor fabricated by Ni-rGOH exhibited higher capacitance and better stability than that of Ni-GOH not annealed at high temperature, probably because of enhanced electrical conductivity and formation of stable NiO species.

2. Experimental

2.1. Preparation of GO

GO was prepared from expandable graphite (Grade 1721, Ashbury Carbon Co. Ltd. USA) by the modified Hummers' method using sulfuric acid (H_2SO_4) and potassium permanganate ($KMnO_4$).[12] All the chemicals used in this study were purchased from Sigma-Aldrich. First, 500 mL of concentrated H_2SO_4 was charged into a 3-L beaker under stirring using a Teflon impeller followed by the addition of 5 g of expanded graphite under stirring at 0 °C after the thermal expansion by 1 min microwave irradiation. Then, 30 g of $KMnO_4$ was added slowly under vigorous stirring, and the solution was maintained for 2 h at 35 °C to oxidize and exfoliate the expanded graphite to individual GO sheets. To complete the oxidation reaction, 6 L deionized water and 50 mL of aqueous hydrogen peroxide (H_2O_2, 30 wt%) were added to that solution. The slurry was washed four times with 10% HCl solution to remove metal ions followed by washing with copious amount of deionized water to completely remove the acid until the pH of the GO suspension reached ~7. In general, the concentration of GO was adjusted to 5–10 mg mL^{-1} in aqueous solution for further experiments.

2.2. Preparation of Ni-GOH and Ni-rGOH

First, 10 mL of aqueous GO solution (5 mg mL^{-1}) was mixed with 50 mg of nickel acetate tetrahydrate under the magnetic stirring followed by the ultrasonic treatment for 1 h at room temperature. Then, the temperature was increased to 80 °C and maintained for 1 day to complete the reaction between GO and Ni ions and form Ni-GOH. The resulting Ni-GOH was freeze-dried at −37 °C for 2 days to remove moisture without destroying the 3D structure. The Ni-rGOH was prepared by the soaking Ni-GOH into ammonium solution for 1 h after drying and heating at 300 °C for 4 h.

2.3. Characterization

X-ray photoelectron spectra were obtained by X-ray photoelectron spectroscopy (XPS) (K-Alpha, Thermo Fisher Scientific ESCALAB 250Xi, USA) using an Al Kα X-ray source. The crystal structure of the samples was characterized by X-ray diffraction (XRD, Rigaku, D/MAZX 2500V/PC, Japan) using a high power X-ray diffractometer equipped with Cu-Kα radiation (35 kV, 20 mA, λ = 1.5418 Å) at a scan rate of 2° (2θ) per min. Bulk structures of the samples were analyzed using the cross-sectional images obtained by field emission-scanning electron microscopy (FE-SEM, JOEL JSM-6500FE, Japan). Thermogravimetric analysis (TGA, TA Instrument, Q50, USA) was used to determine the thermal properties of the samples. Specific surface area and pore structure were analyzed using a surface area and porosity analyzer (Micromeritics, ASAP2020, USA) and calculated using the Brunauer–Emmett–Teller (BET) equation.

2.4. Supercapacitor device and electrochemical test

Ni-GOH and Ni-rGOH were used as the electrodes of supercapacitor devices. The diameter and thickness of electrode were 1 cm and 1 mm, respectively. The electrodes were separated by a glass microfiber filter paper. An aqueous KOH solution (2 M) was used as the electrolyte solution for all the electrochemical tests. Cyclic voltammetry (CV), galvanostatic charge/discharge (CD) curves, and Nyquist plots were measured using an electrochemical workstation (Bio-Logic, SP-50).

3. Results and Discussion

As shown in Fig. 1a, the hydrogel was formed after the hydrothermal process by the reaction between GO sheets and Ni ions with a bulk density of ~43 mg mL^{-1}. Owing to the strong bonding and crosslinking, it can hold as high as 1,400 times of its own weight. The electrostatic force between the negatively charged functional groups such as carboxylic acid and epoxy groups on the GO and positively charged Ni^{2+} ions was the basic reason of the GO gelation, when the nickel acetate solution was added in the GO solution.[13] Under high-temperature condition, the ester linkages between GO and Ni^{2+} ions were formed as described by the following reaction (1):

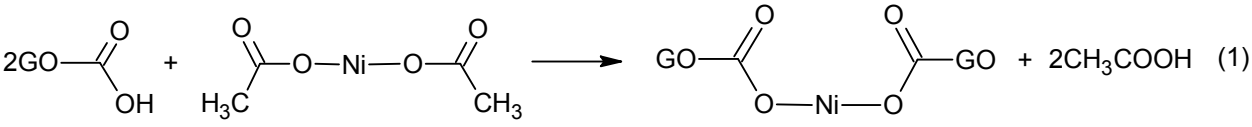

In our experiments, the formation of graphene oxide hydrogel includes 2 steps: (1) gelation by the interaction between Ni ions and GO sheets and (2) reaction at high temperature. The product of first step can be called “gel” and that of second step can be called “hydrogel”. When we varied the concentration of GO solution (0.5, 1, 2, 5 and 7.5 mg/ml), the gelation of GO occurred in all concentrations, but hydrogel was not formed when the concentration of GO was

below 5 mg/ml. The minimum gelation concentration was 0.3 % (w/v) in this study. As the chemical bonds were formed between GO and Ni ions by applying high temperature, the gel was irreversibly crosslinked.

The XRD patterns of Ni-GOH and Ni-rGOH are shown in Fig. 2. The diffraction peaks of Ni-GOH appeared at 11, 34, 36, 41, 59 and 64°, corresponding to the (003), (012), (015), (018), (110) and (113) planes of $Ni(OH)_2$ (JCPDS file No. 14-0117) , respectively,[14] indicating that $Ni(OH)_2$ crystals were also formed by the reaction between Ni^{2+} ions together with a small amount of OH^- ions in the GO solution during the hydrothermal synthesis accompanied by the hydrogel formation by the following reactions. [15]

$$\text{GO-COO}^- + \text{H}_2\text{O} \rightarrow \text{OH}^- + \text{GO-COOH} \quad (2)$$

$$\text{Ni}^{2+} + 2\text{OH}^- \rightarrow \text{Ni(OH)}_2 \quad (3)$$

The GO in the Ni-GOH sample was slowly reduced to rGO by the soaking in ammonium solution at room temperature. After the thermal annealing at 300 °C for 4 h, new peaks appeared at 37, 43 and 64°, corresponding to the (111), (200) and (220) planes, respectively, of NiO (JCPDS file No. 65-2901) in the Ni-rGOH sample.[16] The $Ni(OH)_2$ was decomposed into NiO by the following reaction:[15]

$$\text{Ni(OH)}_2 \rightarrow \text{NiO} + \text{H}_2\text{O} \quad (4)$$

As shown in Fig. S1, the mass loss of Ni-GOH was more than that of Ni-rGOH, also indicating the dehydration of $Ni(OH)_2$ during the thermal annealing.

The broad peak at ~25° corresponds to the re-stacked GO sheets, exhibiting a larger layer-to-layer distance than that of graphite because of the presence of functional groups and captured water molecules.[7]

The morphology of Ni-rGOH was investigated by SEM, and the images are shown in Fig. 3a. Ni-rGOH exhibited a well-developed highly porous structure. Both the wrinkled rGO and smoothly surfaced NiO were observed, indicating that Ni ions contributed to the formation of $Ni(OH)_2$ structures as well as 3D GOH networks during the hydrothermal process. The 2D Raman mapping and TEM images also confirmed the SEM results as shown in Fig. S2 and S3. The energy dispersive X-ray spectra (EDS) shown in Fig. S4 and Table S1 indicate that a relatively small amount of Ni (~3.9 atomic%) was present in Ni-rGOH.

The N_2 adsorption–desorption isotherm of Ni-rGOH is shown in Fig. 3b. The BET surface area of Ni-rGOH was 132 m^2 g^{-1}, which is several times higher than that of pure NiO nanoparticles.[17] The increased surface area was attributed to the formation of 3D structure with GO by the chemical crosslinking during the one-pot hydrothermal process. The shape of N_2 adsorption–desorption isotherm indicates type H2, owing to the formation of a mesoporous structure connected or nonconnected ink-bottle pores or cavities in the hydrogel structure.[7]

The chemical structures of the samples fabricated in this study were determined by XPS as shown in Fig. 4a. Both the Ni-GOH and Ni-rGOH exhibited characteristic peaks of C 1s, O 1s, and Ni 2p in the survey spectra. The increased relative intensity of carbon compared to oxygen indicates the reduction of the functional groups of GO during the high-temperature annealing. High resolution C 1s peaks of Ni-GOH and Ni-rGOH were deconvoluted into C–C/C=C, C–O, C=O, and O–C=O bonds at the binding energies of 284.65, 285.4, 286.4, and 288.9 eV, respectively, by a Gaussian function, as shown in Fig. 4b.[18] The intensity of the C–O, C=O and O–C=O peaks of Ni-rGOH was lower than that of Ni-GOH because of the reduction of functional groups. Interestingly, the intensity of C–O peak of Ni-GOH was lower than that of GO because of the loss of functional groups during the reaction between GO and Ni ions,

whereas the O–C=O intensity of Ni-GOH was higher than that of GO (Fig. S5), probably because of a transesterification reaction between the hydroxyl groups of GO and ester groups of nickel acetate as described in the following reaction (2):[19]

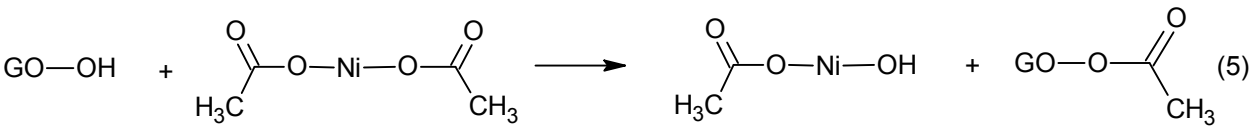

(5)

As shown in Fig. 4c, the high-resolution XPS peak of O 1s of Ni-GOH and Ni-rGOHs was deconvoluted into three sub-peaks centered at 529.9, 531.4, and 532.7 eV, corresponding to fully coordinated oxygen species to carbon or nickel atoms, oxygen atoms in the vicinity of an oxygen vacancy, and hydroxyl groups (C–OH), respectively.[20] The peak position and intensity were maintained even after the high-temperature annealing, indicating that there was not a noticeable change in Ni–O bonds during the heat treatment. The high-resolution XPS peaks of Ni 2p of NiO and $Ni(OH)_2$ shown in Fig. 4d show that NiO peak appeared at ~854 eV, and there is a small shift in the satellite peak toward higher binding energy after the thermal annealing as reported in other study.[21]

The electrochemical properties of Ni-GOH and Ni-rGOH were determined by the CV and galvanostatic charge–discharge systems. The specific capacitance was calculated from both the CV and CD by Eqs. (6) and (7), respectively.[22]

$$C_{S,V} = \frac{\int idV}{2 \times m \times \Delta V \times S} \quad (6)$$

where $C_{S,V}$ is the specific capacitance measured from CV, $\int idV$ is integrated area of the CV curve, m is the mass of the single electrode, ΔV is the potential range, and S is the scan rate,.

$$C_{S,D} = \frac{I}{m \times dV/dt} \quad (7)$$

where $C_{S,D}$ is the specific capacitance measured from CD, I is constant current density, and dV/dt is the slope of the discharge curve,.

As shown in Fig. 5, Ni-GOH and Ni-rGOH exhibits redox current peaks of $Ni(OH)_2$ and NiO with electrolyte, respectively, corresponding to the $Ni(OH)_2$/NiOOH (A_1/A_2) and NiO/NiOOH (B_1/B_2) redox couples according to Eqs. (8) and (9): [15, 23]

$$Ni(OH)_2 + OH^- \leftrightarrow NiOOH + H_2O + e^- \quad (8)$$

$$NiO + OH^- \leftrightarrow NiOOH + e^- \quad (9)$$

The specific capacitances of Ni-GOH and Ni-rGOH were calculated based on the CV curves at various scan rates and CD curves at various current densities (Fig. S6), as listed in the Tables 1 and 2. The Ni-rGOH exhibited 20–50% higher specific capacitance than that of Ni-GOH, probably because of the increased conductivity of GOH networks, and the transformation of $Ni(OH)_2$ to NiO in the hydrogel structure after the thermal-annealing process.[24] Interestingly, the capacitance of Ni-rGOH was much higher than that of high surface area GOH fabricated by ethylene diamine, attributed to the of redox current of NiO formed in the GOH network.[7] The Nyquist plots of Ni-GOH and Ni-rGOH measured by the electrochemical impedance spectroscopy (EIS) are shown in Fig. 5c. At a high frequency, the smaller diameter of the semicircle of Ni-rGOH than that of Ni-GOH indicates the smaller charge transfer resistance of Ni-GOH electrode.[25] At a low frequency, Ni-GOH and Ni-rGOH exhibited the similar slopes, indicating the similar ion diffusion/transport in the KOH electrolyte, robust 3D morphology, and pore structure maintained during the thermal annealing process.

Two important parameters of the performance of asymmetric supercapacitor, the energy density (E_s) and power density (P_s), were calculated by the following equations:[11]

$$E_s = \frac{1}{2} C_s U^2 \quad (10)$$

$$P_s = 3600\frac{E_S}{t} \quad (11)$$

where C_s is the specific capacitance, U is the operating voltage of device, and t is the discharge time. The Ragone plots shown in Fig. 5d also indicate that Ni-rGOH shows high energy density of 175.5 Wh kg^{-1} at a power density of 1.125 kW kg^{-1}, while maintaining a high energy density of 118 Wh kg^{-1} at a power density of 4.5 kW kg^{-1}, which is 20–30% higher than those of Ni-GOH and several folds higher than those of the rGO-Ni-Co oxide based-electrode reported previously.[26] The stability of Ni-GOH and Ni-rGOH electrodes was investigated by CV after 1,000 cycles at a scan rate of 50 mV s^{-1}. The specific capacitance was maintained at 89% and 91% for Ni-GOH and Ni-rGOH, respectively. A slightly higher electrochemical stability of Ni-rGOH was attributed to the more stable nature of NiO than $Ni(OH)_2$.

4. Conclusions

GOH was prepared using Ni ions as the linkages between the graphene oxide sheets by a simple hydrothermal method. Owing to the formation of 3D networks, the GOH fabricated in this study exhibited a low bulk density and high surface area. The Ni-rGOH exhibited highly enhanced capacitance than that of GOH attributing to the NiO redox cycle. After the thermal annealing and chemical reduction, $Ni(OH)_2$ and GO were converted into NiO and rGO, respectively, thus improved the electrochemical performances by the enhanced stability and reduced resistance.

Acknowledgments

This research was supported by Basic Science Research Program through the National Research Foundation of Korea (NRF) funded by the Ministry of Education (2013R1A1A2A10004468).

Notes and references

1 C. G. Liu, Z. N. Yu, D. Neff, A. Zhamu and B. Z. Jang, *Nano Lett*., 2010, **10**, 4836-4868.

2 P. Simon and Y. Gogotsi, *Nat. Mater*., 2008, **7**, 845–854.

3 G. Yu, L. Hu, N. Liu, H. Yang, M. Vosgueritchian, Y. Yang, Y. Cui and Z. Bao, *Nano. Lett.,* 2011, **11**, 4438–4442.

4 H. Wang, H.S. casalongue, Y. Liang and H. Dai, *J. Am. Chem. Soc.,* 2010, **132**, 7472-7477.

5 L. L. Zhang and X. S. Zhao, *Chem. Soc. Rev*., 2009, **38**, 2520–2531.

6 G. Wang, L. Zhang and J. Zhang, *Chem. Soc. Rev*., 2012, **41**, 797–828.

7 V.H. Luan, H.N. Tien, L.T. Hoa, N.T.M. Hien, E.S. Oh, J.S. Chung, E.J. Kim, W.M. Choi, B.S. Kong and S.H. Hur, *J. Mater. Chem. A*, 2013, **1**, 208–211.

8 B. Adhikari, A. Biswas, and A. Banerjee, *ACS Appl. Mater. Interfaces*, 2012, **4**, 5472−5482.

9 Y. Xu, K. Sheng, C. Li and G. Shi, *ACS Nano*, 2010, **4**, 4324–4330.

10 H. Wang, H. Yi, X. Chen and X. Wang, *J. Mater. Chem. A*, 2014, **2**, 3223–3230.

11 F. Luan, G. Wang, Y. Ling, X. Lu, H. Wang, Y. Tong, X.X. Liu and Y. Li, *Nanoscale*, 2013, **5**, 7984–7990.

12 W.S. Hummer and R.E. Offeman*, J. Am. Chem. Soc*., 1958, **80**, 1339–1339.

13 S. Park, K.S. Lee, G. Bozoklu, W. Cai, S. T. Nguyen and R.S. Ruoff, *ACS nano*, 2008, **2**, 572–578.

14 X. Liu, y. Zuo, X. Huang and G. Li, *RSC Adv*., 2014, **4**, 6397–6406.

15 X. Xia, Y. Yang, D. Chao, C. Guan, Y. Zhang, L. Li, X. Ge, I.M. Bacho, J. Tu and H.J. Fan, *Nanoscale*, 2014, **6**, 5008–5048.

16 G. Li, X. Wang, H. Ding and T. Zhang, *RSC Adv*., 2012, **2**, 13018–13023.

17 A.G. Al-Sehemi, A.S. Al-Shihri, A. Kalam, G. Du and T. Ahmad, *J. Mol. Struct*., 2014, **1058**, 56–61.

18 D. Yang, A. Velamakanni, G. Bozoklu, S. Park, M. Stoller, R. D. Piner, S. Stankovich, I. Jung, D. A. Field, C. A. Ventrice Jr. and R. S. Ruoff, *Carbon,* 2009, **47**,145–152.

19 A. K. Singh and S. D. Fernando, *Chem. Eng. Technol*., 2007, **30**, 1716–1720.

20 C. Y. Koo, K. K. Song, Y. H. Jung, W. S. Yang, S. H. Kim, S. H. Jeong and J. H. Moon, *ACS Appl. Mater. Interfaces*, 2012, **4**, 1456–1461.

21 M.C. Biesinger, B.P. Payne, L.W.M. Lau, A. Gerson and R.St.C. Smart, *Surf. Interface Anal*., 2009, **41**, 324–332.

22 A. Yu, I. Roes, A. Davies and Z. Chen, *Appl. Phys. Lett.*, 2010, **96**, 253105 1–3.

23 P. Subramanian, J. Niedziolka-Jonsson, A. Lesniewski, Q. Wang, M.Li, R. Boukherroub and S. Szunerits, *J. Mater. Chem. A*, 2014, **2**, 5525–5533.

24 V. Srinivasan and J. W. Weidner, *J. Electrochem. Soc*., 2000, **147**, 880–885.

25 G.P. Kim, I. Nam, N.D. Kim, J. Park, S. Park and J. Yi, *Electrochem. Commun*. 2012, **22**, 93–96.

26 X. Wang, W.S. Liu, X.H. Lu and P.S. Lee, *J. Mater. Chem*., 2012, **22**, 23114–23119.

Table 1 Specific capacitances of Ni-GOH and Ni-rGOH measured by CV at various scan rates.

Scan rates/mV s^{-1}	**10**	**50**	**100**
Ni-GOH /F g^{-1}	272	203	168
Ni-rGOH /F g^{-1}	323	258	250

Table 2 Specific capacitances of Ni-GOH and Ni-rGOH measured by the galvanostatic charge–discharge (CD) at various current densities.

Current density/A g^{-1}	**0.625**	**1.25**	**2.5**
Ni-GOH /F g^{-1}	273	218	195
Ni-rGOH /F g^{-1}	351	309	237

Figure Captions

Figure 1 (a) Schematic representation of Ni-GOH fabrication steps and (b) optical images of the Ni-GOHs.

Figure 2 XRD patterns of Ni-GOH and Ni-rGOH.

Figure 3 (a) Cross-sectional SEM images and (b) nitrogen adsorption–desorption isotherms of Ni-rGOH.

Figure 4 (a) XPS survey and high-resolution XPS spectra of (b) C 1s, (c) O 1s, and (d) Ni 2p peaks of Ni-GOH and Ni-rGOH.

Figure 5 Electrochemical properties of Ni-GOH and Ni-rGOH electrodes in supercapacitor: (a) the CV curves at a scan rate 100 mV s^{-1} and (b) the CD curves at 2.5 A/g, (c) the Nyquist plot at a DC bias of 0.7 V and the frequency range from 0.01 Hz to 100 kHz, and (d) the Ragone plot.

Figure 6 Cycling performance of Ni-GOH and Ni-rGOH during 1,000 cycles at a scan rate of 50 smV s^{-1}.

Figure 1

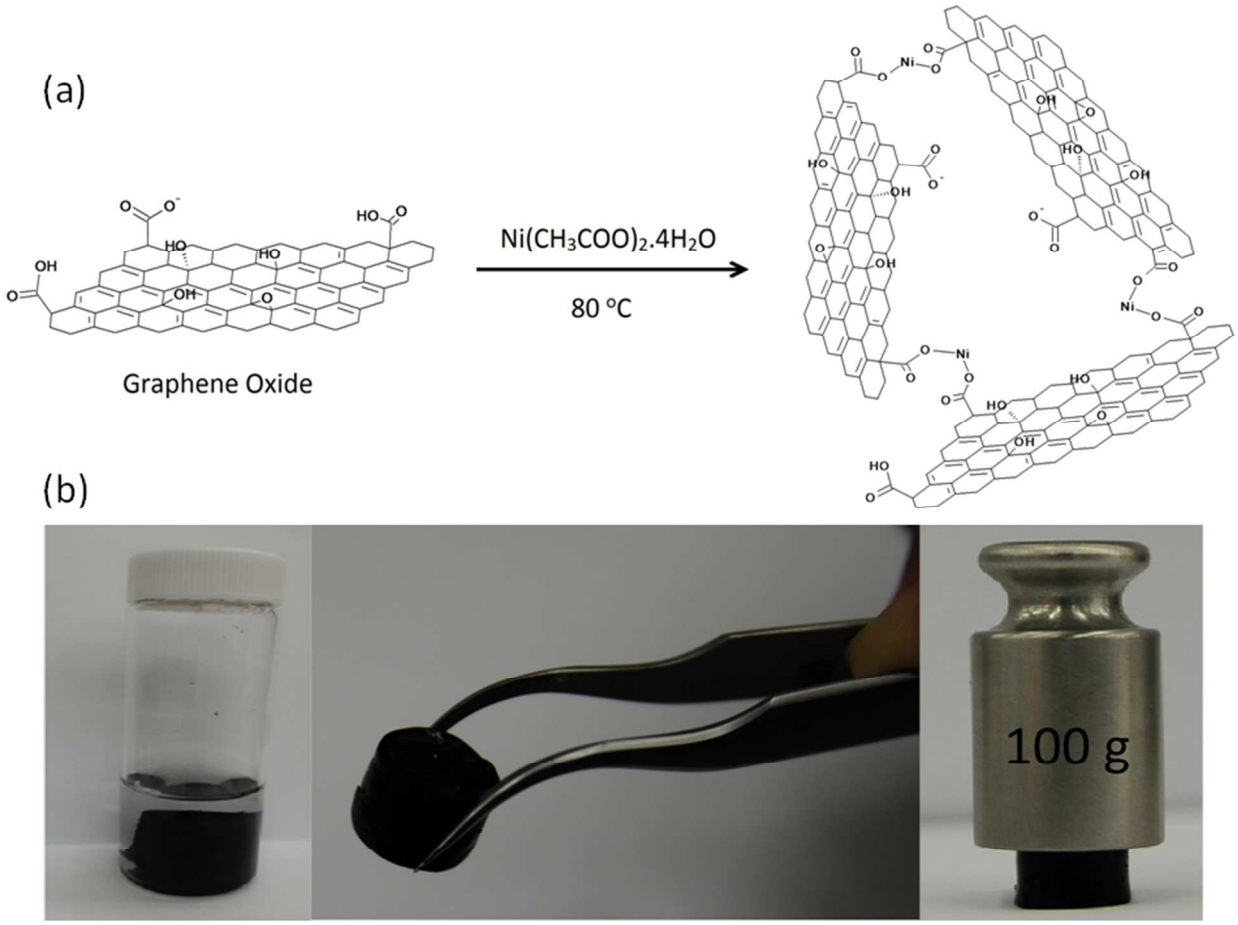

Figure 2

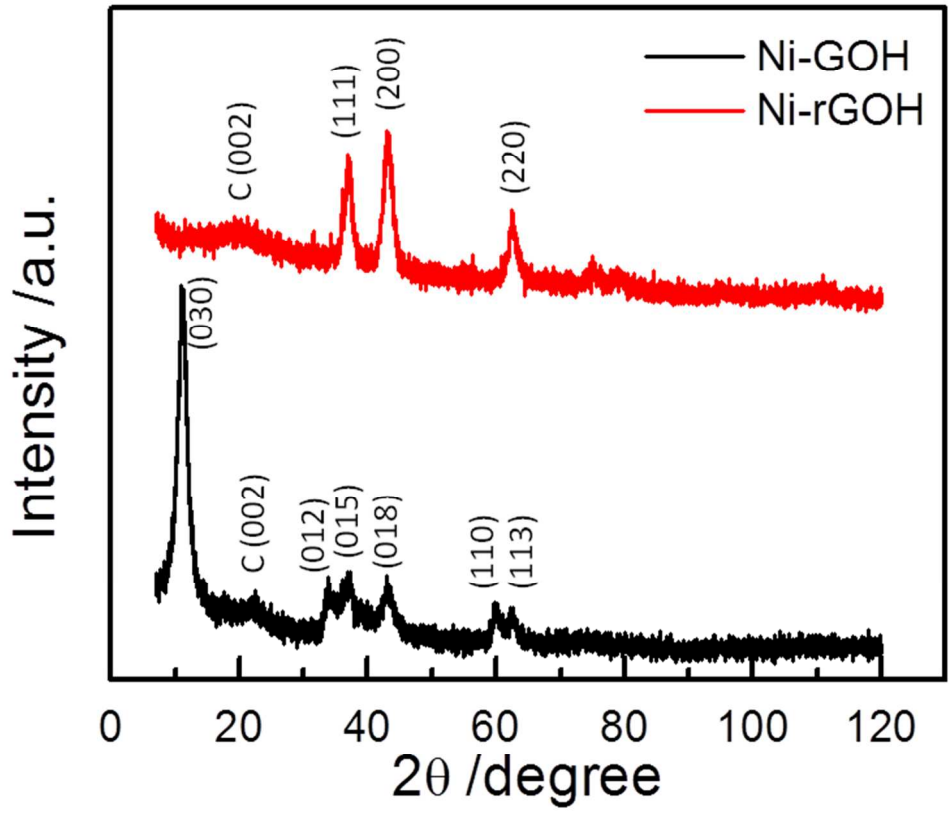

Figure 3

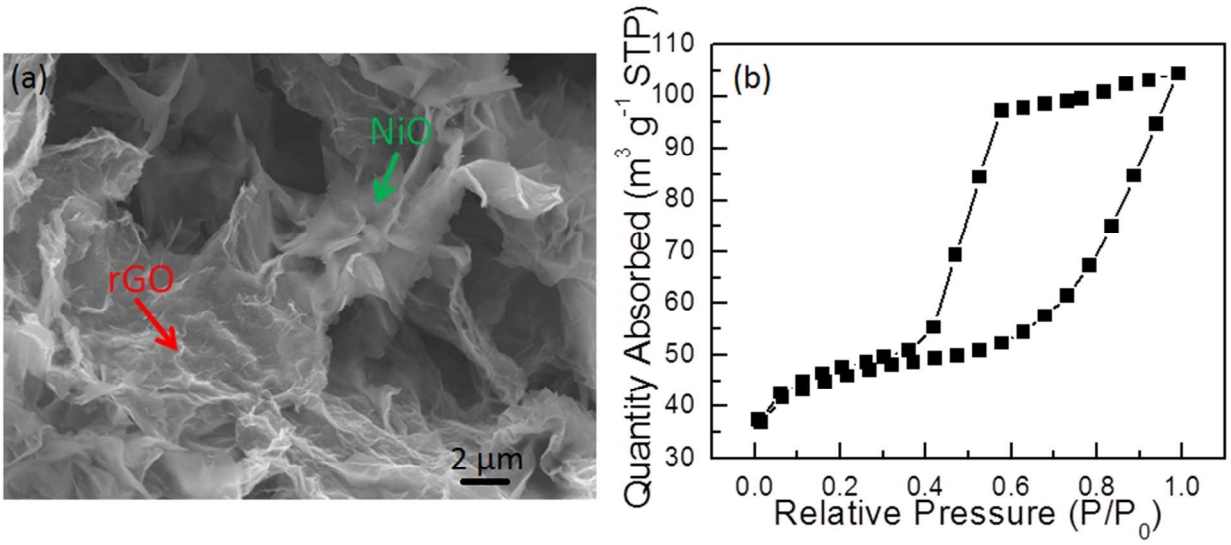

Figure 4

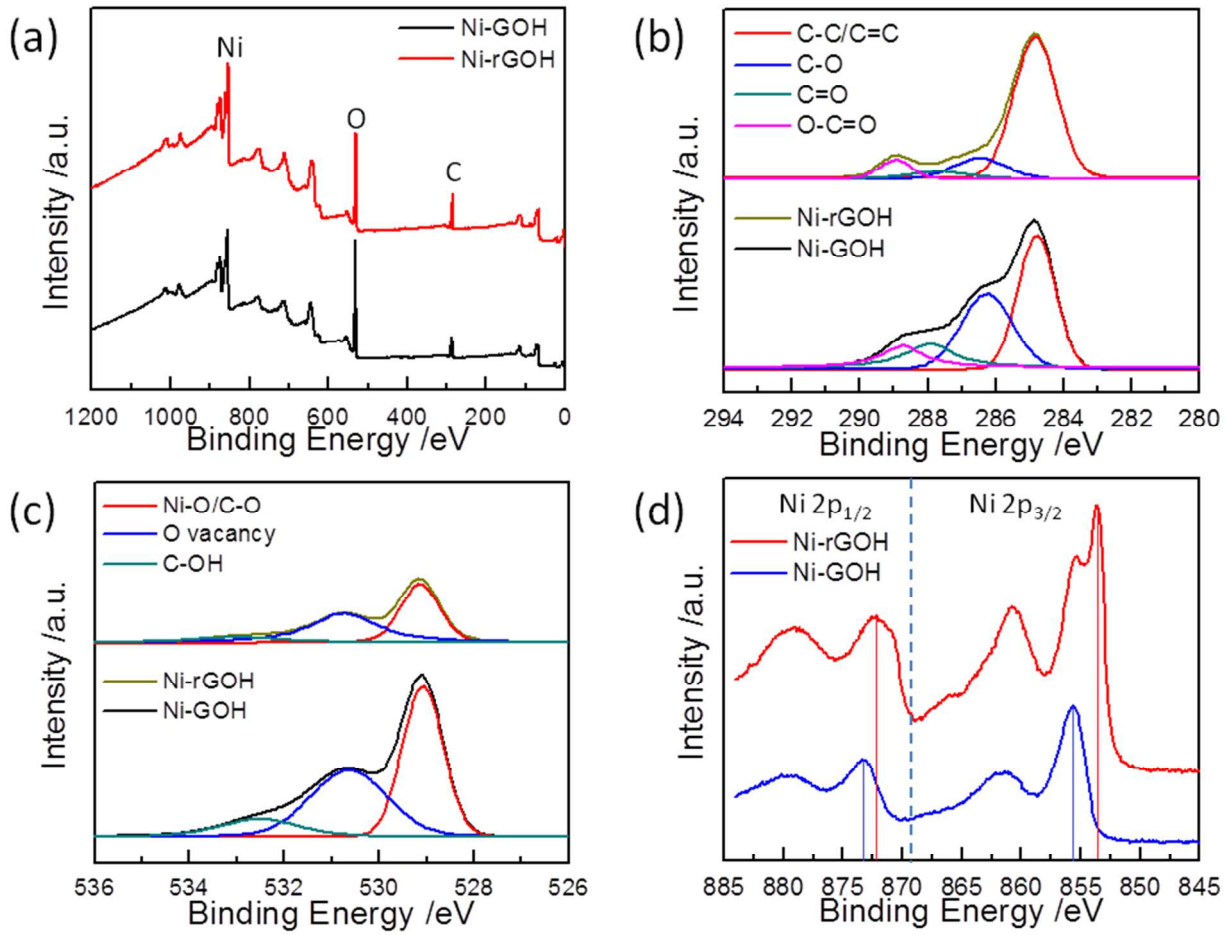

Figure 5

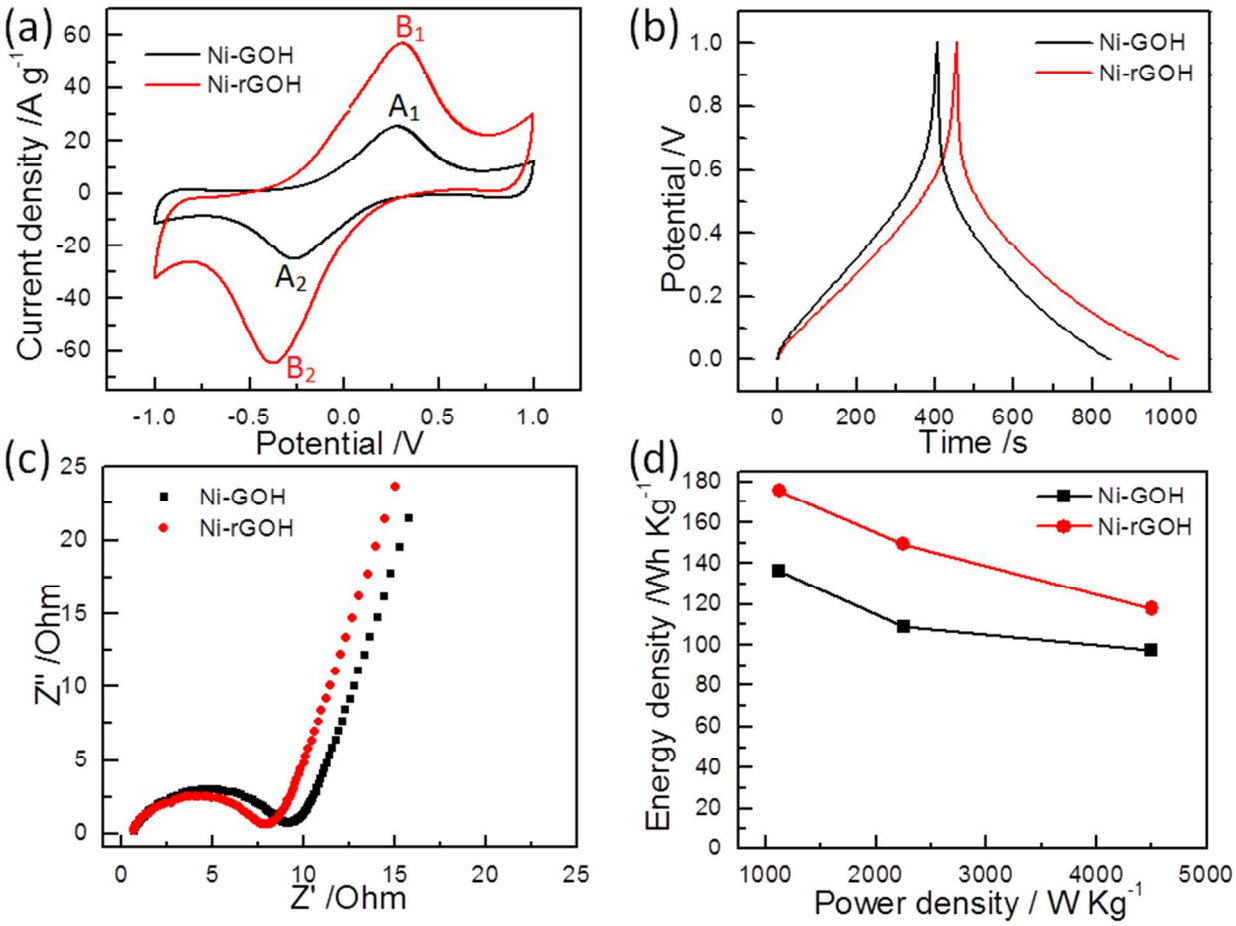

Figure 6